Ceramics International 47 (2021) 2793–2801

Contents lists available at ScienceDirect

Ceramics International

journal homepage: www.elsevier.com/locate/ceramint

New, tough and strong lithium metasilicate dental glass-ceramic

Viviane O. Soares [a,*], Francisco C. Serbena [b], Ivan Mathias [c], Murilo C. Crovace [d], Edgar D. Zanotto [d]

[a] Department of Sciences, State University of Maringá (UEM), CEP 87360-000, Goiorè, PR, Brazil
[b] Department of Physics, State University of Ponta Grossa (UEPG), CEP 84030-900, Ponta Grossa, PR, Brazil
[c] Department of Mathematics, State University of Ponta Grossa (UEPG), CEP 84030-900, Ponta Grossa, PR, Brazil
[d] Vitreous Materials Laboratory (LaMaV), Department of Materials Engineering (DEMa), Federal University of São Carlos (UFSCar), CEP 13565-905, São Carlos, SP, Brazil

ARTICLE INFO

Keywords:
Dental
Glass-ceramic
Mechanical properties
Toughness

ABSTRACT

Glass-ceramics have found widespread use in dentistry due to their favorable properties: biocompatibility, chemical inertness, high fracture strength and toughness, superior esthetics, color stability, and translucence. The objective of this work was to develop a new tough, strong and machinable glass-ceramic based on the lithium metasilicate (LS) crystal phase. We designed a glass composition aimed to yield LS crystals after proper treatment. We melted, casted, and crystallized the glass for a favorable microstructure. We then characterized its microstructure and relevant mechanical, optical and chemical properties with several experimental tools. We also measured the residual stresses. This newly developed glass-ceramic shows a house-of-cards microstructure composed of 50% vol. plate-like LS crystals of 5–25 μm, randomly dispersed in a glassy matrix. Lithium disilicate (12% vol.), two minor crystal phases, and 34% vol. residual glass are also present. The average fracture toughness measured by the double torsion technique is 3.5 ± 0.5 MPa $m^{1/2}$. The average fracture strength, evaluated by the ball-on-three balls (B3B) technique, is 450 ± 40 MPa. The elastic modulus, determined by nanoindentation, is 124 ± 2 GPa, the linear thermal expansion coefficient is 13.6 × 10^{-6} $°C^{-1}$, and the solubility in 4%vol. acetic acid is 215 ± 30 μg/cm^2, which is below the limit established by the ISO 6872 standard for some applications, but improper for uncoated use. These properties could still be optimized. The improved toughness, strength, and reasonable machinability indicate that, after optimization, this glass-ceramic could be a very promising candidate for dental restorative applications.

1. Introduction

Glass-ceramics (GCs) are inorganic, non-metallic materials prepared by controlled crystallization of glasses via different processing methods. They contain at least one type of functional crystalline phase and a residual glass. The crystallized volume fraction may vary from ppm to almost 100% [1]. GCs have become popular in dentistry because of their biocompatibility, chemical inertness, high fracture strength and toughness, superior esthetics, color stability, translucency and machinability. The development and use of GCs for dental applications have been thoroughly described in Ref. [2,3].

With the advance in computer-aided design and computer-aided manufacturing technology (CAD/CAM) [4,5], ceramic dental restorations can be machined from a solid ceramic block instead of multiple conventional firings of feldspathic porcelain or injected into a mold at high temperature by hot-pressing. The main advantage of the CAD/CAM technique is to precisely reproduce the shape and size of the prosthesis, which leads to a final piece with minimal defects or flaws ensuring better mechanical properties than conventional porcelains [6,7].

The first glass-ceramic (GC) specifically developed for dental applications was based on tetrasilic mica, $KMg_{2.5}Si_4O_{10}F_2$ (DiCOR ®, Corning Inc./Dentsply Int.) [8]. This type of GC was used to produce dental restorations by the injection molding technology. Further investigations and improvement on this material led to a product that could be processed using CAD/CAM technology.

The lithium disilicate (LS2) machinable GCs for CAD/CAM restoration were launched in the dental market around 2005 [2,9]. Nowadays, they are widely used in dental clinics due to their high chemical durability, strength and toughness combined with superior aesthetics, which ensure a tooth-like appearance [10]. The machinable type lithium

* Corresponding author.
E-mail addresses: vosoares@uem.br, soares.v.o@gmail.com, vosoares@uem.br, soares.v.o@gmail.com (V.O. Soares).

https://doi.org/10.1016/j.ceramint.2020.09.133
Received 27 June 2020; Received in revised form 2 September 2020; Accepted 13 September 2020
Available online 19 September 2020
0272-8842/© 2020 Elsevier Ltd and Techna Group S.r.l. All rights reserved.

disilicate GCs are machined in a pre-crystallized step, when the piece contains around 40% vol. of lithium metasilicate (LS) crystals. It is then crystallized to form 60–70%vol needle-like disilicate crystals. This final heat treatment ensures translucency, appropriate color, chemical durability and strength to the prosthesis [11]. The intricated microstructure is accountable for the excellent fracture strength and toughness. Commercial machinable dental GCs have a fracture strength of ~360 MPa (biaxial flexure) and fracture toughness (SENV) from 2.0 to 2.5 MPa $m^{1/2}$ [9,12–14].

In this research, we developed a new GC based on the Li_2O–SiO_2 system having approximately 50% vol. LS crystals, which yielded high toughness and strength, as well as translucency, and some degree of machinability to the GC. The continuous search for GCs with greater toughness, fracture strength, machinability and improvement of the processing technique (one-step crystallization and machining) was the driving force behind our effort to obtain this material.

2. Experimental procedure

A glass with the chemical composition (mol%): 52.5 SiO_2; 39.9 Li_2O; 0.8 P_2O_5;1.4 TiO_2; 1.4 CaO; 1.6 B_2O_3; 0.6 K_2O; 0.6 Al_2O_3; 0.4 ZrO_2; 0.4 ZnO; 0.2 SrO; 0.2 BaO was obtained from analytical-grade chemicals. The main differences between this glass composition and the commercial compositions are the higher amount of Li_2O used (around 40 mol %) and the lack of coloring agents or rare earth elements. The mixture of precursor powders was melted in a platinum crucible at 1250 °C for 4 h in an electrical furnace. The melts were poured between two stainless steel plates every 1 h, crushed and re-melted three times to homogenize the liquid. Finally, they were cast in a stainless-steel mold, and the resulting glass pieces (cylinders of 12 mm in diameter, and bars of 15 × 30 × 3 mm^3 and 30 × 50 × 2 mm^3) were annealed at 400 °C for 2 h for stress relief.

Differential scanning calorimetry (DSC) experiments were carried out using small pieces in a Netzsch DSC 404 equipment to determine the characteristic temperatures of the glass, with a heating rate of 10 °C. min^{-1} up to 1150 °C. After preliminary screening, we picked one particular composition for detailed characterization, as explained below.

To obtain GCs, glass pieces were heat-treated in a tubular electrical furnace, with a variation of ±1 °C. The selected heat treatment was 5 min at 455 °C for nucleation and 3 min at 800 °C for crystal growth. Longer nucleation treatments lead to smaller crystals; for instance, nucleation for 24 h results in crystal sizes < 5 μm. The samples were cooled inside the annealing furnace using a cooling rate of approximately 15 °C.min^{-1}. The GCs were subsequently ground with SiC abrasive papers of different granulometries down to a 1200 grit, and then polished using a fine suspension of CeO_2 in water. Scanning electron microscopy (SEM, Phillips FEG) was used to observe the microstructure before and after etching by a 5 vol% HF solution for 10 s.

Before any mechanical testing, such as hardness, all samples were annealed at 440 °C for 2 h and cooled at a rate slower than 1 °C.min^{-1} to room temperature to relieve any surface residual stress caused by the grinding procedure. The internal residual stresses owing to the thermal expansion coefficient (TEC) mismatch between the crystals and the residual glass phases are permanent and cannot be eliminated. We will address these stresses later on in this article.

The crystalline volume fraction was determined by X-ray diffraction. α-alumina powder (99% purity, grain size < 3 μm, Alcoa) was mixed to a powdered sample in a 1:1 proportion by weight. The diffractograms were recorded using CuKα radiation and were measured in the θ–θ geometry at room temperature using a Rigaku Ultima IV diffractometer in the Bragg-Brentano geometry. The 2θ range was scanned from 10 to 80°, with a step size of 0.02° in the 2θ scale, 10 s for each step. The volume fraction of the crystalline phases and alumina were determined by Rietveld refinement of the XRD patterns where the amorphous glass contribution was considered as part of the background. Rietveld refinement of the crystal structures was performed using the GSAS program [15] with the EXPGUI interface [16] and the TOPAS-Academic software [17]. Using the known amount of alumina added to the powdered GC and its estimated volume fraction obtained by Rietveld refinement, a simple rule of mixture allowed us to calculate the volume fractions of each crystalline phase and of the residual glass.

The hardness (H) and elastic modulus (E) of the GC were measured using instrumented indentation with a Nanoindenter XP indenter (MTS Instruments) with a Berkovich diamond tip. The maximum applied load was 400 mN in 10 loading-unloading cycles. A matrix of 25 indentations was made in each sample, and the values of H and E were calculated following the procedure proposed by Oliver and Pharr [18]. Therefore, the values of H and E are the averages of all indentations.

The fracture strength was measured using a ball-on-three-balls (B3B) apparatus [19,20] using three 4 mm (radius) alumina balls under the samples and a fourth ball centralized on the upper surface of the samples. The jig was made of stainless steel. The tests were carried out using a universal testing machine (AGS-5 kN, Shimadzu) with a displacement rate of 1 mm min^{-1} at 80% relative humidity. The samples had a disk format with 12 mm in diameter and 1.2 ± 0.1 mm thickness, a total of 11 samples were tested. In this work, all samples were polished using a 1200 grit SiC paper, which corresponds to a grain size of 15 μm, followed by annealing at 440 °C for 35 min and a furnace cooled to room temperature at a rate of 2 °C.min^{-1} for stress relief from the polishing process.

The biaxial fracture strength, σ, was calculated by Ref. [20]:

$$\sigma = f(R, R_c, t, \nu)\frac{P}{t^2}, \quad (1)$$

where f is a dimensionless factor, which depends on the sample radius (R), ball radius (R_c), sample thickness (t), and sample Poisson's ratio (ν), and P is the failure load. A minimum of 9 GC samples were tested.

The fracture toughness (K_{DTIC}) of the GC samples was measured using the double torsion technique at room temperature in air as described in Refs. [21]. Seven plates of 30 × 15 × 1.5 mm^3 were cut and their surfaces were ground and subjected to polishing in a CeO_2 water suspension to obtain parallel faces. A 10 mm long 450 μm wide notch was introduced using a diamond disk. Samples were stress relieved before and after introducing the notch by annealing at 440 °C for 2 h and cooled at a rate slower than 1 °C.min^{-1}. An initial crack was produced by a 10 N Vickers indentation near the notch tip, which was subsequently propagated at a displacement rate of 0.01 mm min^{-1}, to promote crack growth. The testing apparatus consisted of a jig in a universal testing machine (Shimadzu AGS-X 5 kN). The jig consisted of four stainless steel spheres, all 3 mm in radius, fixed onto a plate and separated by 11 mm in width and 20 mm in length. An alumina sphere with a 5 mm radius was placed between the edges of the notch and used to apply the compression load, forming a bending arm with the lower spheres of 5.5 mm. The load was applied at a displacement rate of 2 mm min^{-1}.

The fracture toughness was calculated using the method described in Ref. [22,23]:

$$K_{DTIC} = P_C W_m \sqrt{\frac{3}{Wt^4(1-\nu)\psi}}, \quad (2)$$

where W_m is the moment arm, P_C is the load at fracture, t is the sample thickness, ν is the Poisson ratio, and ψ is equal to 1–0.6302τ + 1.20τ.exp(-π/τ), where τ = 2 t/W.

Surface scanning profiles of the fractured surfaces of the double torsion test samples were obtained using a laser confocal microscope (LEXT OLS4100) with a 20x objective lens. These profiles were measured on six different regions of the fractured surface. They were 250 μm in length. The crack angle at each point was determined based on the profile derivative, similar to the study reported in Ref. [24], and

was calculated as arctan[Δy/Δx], where Δy is the difference in height between two neighbor measurement points separated by the step Δx. The step Δx was 0.25 μm.

The TEC of the glass and the GC were determined using a Netzsch DIL 402 (Netzsch, Selb, Germany) PC dilatometer and a heating rate of 5 °C. min^{-1} in air. Samples of 3 × 2x40 mm^3 were prepared by cutting and polishing them to obtain parallel faces.

The residual stresses in the crystalline phases were measured by X-ray diffraction (XRD). The experimental conditions were the same as described earlier. A stress-free reference powder sample was prepared by crushing a bulk sample in an agate mortar, sieving, and annealing at 440 °C for 30 min, followed by slow cooling to room temperature. The average particle size measured by laser scattering using a Horiba LA930 device was 8 μm. The anisotropic strains ε_i in each phase were calculated from the change of the unit cell parameters of each crystalline phase by comparing bulk (stressed) and powder (stress-free) samples [25,26] as $\Delta a/a_0$, where Δa is the difference between the crystal unit cell dimension in the bulk and powder samples along a particular crystallographic direction *i*, and a_0 is the unit cell parameter of the powder sample in that specific direction, as calculated by the Rietveld refinement. The average strain $\overline{\varepsilon}$ in each phase was calculated as $(\varepsilon_a+\varepsilon_b+\varepsilon_c)/3$. The average stress $\overline{\sigma}_{exp}$ in each phase was obtained from Hooke's law as $\overline{\sigma}_{exp} = E_i/(1-2\nu_i).\overline{\varepsilon}$.

A spectrophotometer (Lambda 1050; Perkin Elmer) with an integrating sphere was used to evaluate the total transmittance of light in percentage (T_t%). Measurement conditions were set as follows: wavelength range of 380–780 nm, bandwidth 4.0 nm, scan speed 60 nm min^{-1}, data interval 1.0 nm, and a xenon light source. The new GC was compared to commercial lithium disilicate GCs: IPS e.max Press A1 High Translucency (Press A1 HT); IPS e.max Press A3 Low Translucency (Press A3 LT); IPS e.max Press A3 Medium Opacity (Press A3 MO) produced by Ivoclar Vivadent. The samples were cut from each block with a diamond wheel, ground with a surface grinding sheet (220 up to 1200 mesh), and polished with diamond paste (3–0.25 μm) to produce thicknesses of 0.95 ± 0.02 mm. The T_t% values at the wavelength of 555 nm were used to compare the specimens. Since the human eye is most sensitive to 555 nm, this wavelength is used by the CIE and JIS. Therefore, we selected this wavelength based on the definition of the International Commission on Illumination (CIE S 017) [27] and the Japanese Industrial Standard (JIS Z 8113) [28].

The machinability of the designed GC was only qualitatively evaluated. A sample of 12 × 18 × 20 mm^3 was prepared and machined using a CAD/CAM system (Cerec inLab Sirona®) using their standard milling program to obtain a molar tooth, chosen due to its high complexity.

The chemical durability was determined according to the ISO 6872 [29]. Three samples of 30 × 50 × 2 mm^3 were prepared and washed in deionized water, dried at 150 °C for 4 h and weighed on a balance accurate to 0.1 mg. Each sample was immersed in a 4%vol. acid acetic solution at 80 °C for 16 h, using 100 ml of the solution to 30 cm^2 of exposed surface area. Then, the samples were washed, dried at 150 °C for 4 h, and weighed again. The mass loss was calculated in micrograms per square centimeters.

3. Results

The DSC curve of the selected parent glass is shown in Fig. 1. The glass transition temperature (T_g) is 443 °C, the temperature of the first crystallization peak (T_{c1}) is 589 °C, and the temperature of the second crystallization peak (T_{c2}) is 750 °C. Three endothermic peaks are observed at 905 °C, 965 °C and 1080 °C, and can be attributed to the melting of the crystalline phases. The liquidus temperature is thus somewhat above 1080 °C. The optimized heat treatment to obtain the GC was 455 °C during 5 min for nucleation, 800 °C for 3 min for crystal growth, followed by cooling at 15 °C.min^{-1}.

The resulting microstructures are shown in Fig. 2. Fig. 2(a) shows a polished surface of the GC after severe chemical etching in HF, with a

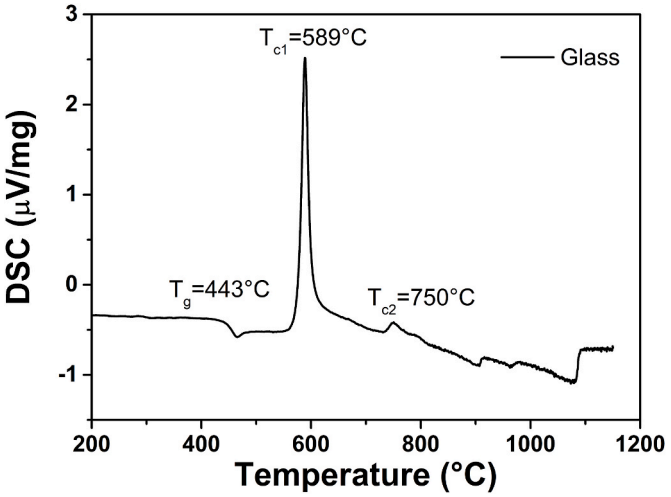

Fig. 1. DSC curve of the selected parent glass (bulk sample), using a heating rate of 10 °C.min^{-1}.

"house-of-cards", i.e., a network of plate-like interlocked LS crystals. The size of the plates is in the range of 5–25 μm, with an average length of 9 ± 3 μm. Fig. 2(b) and (c) show BSE images of the polished GC surface. The microstructure consists of large plate-like LS crystals (1), smaller rounded LS2 crystals (2), LS crystals (3) and the residual glass (4). Several 1–2 μm microcracks or smaller, indicated by arrows in Fig. 2(b), are observed along the LS2 crystal-glass interfaces and in the residual glass.

Fig. 3 shows the XRD pattern of the GC mixed with α-alumina for phase quantification. The crystalline phases identified are alumina (Al_2O_3), lithium metasilicate (Li_2SiO_3), lithium disilicate ($Li_2Si_2O_5$), lithium phosphate (Li_3PO_4) and α-quartz (SiO_2). The crystallized volume fractions in the GC determined by Rietveld refinement are: 50 ± 2 % Li_2SiO_3, 12.5 ± 0.9 % $Li_2Si_2O_5$, 1.9 ± 0.3 % Li_3PO_4, 1.9 ± 0.3 SiO_2 and 33.7 ± 2 % residual glass.

The hardness (H) and elastic modulus (E) were determined by instrumented indentation as a function of the contact depth. At the deepest contact depth, they are 6.9 ± 0.5 GPa and 124 ± 2 GPa, respectively. The developed GC has values of hardness and elastic modulus higher than those of other dental GCs [25,26,30,31]. Commercial lithium disilicate GCs, for example, usually have a hardness in the 5.0–7.0 GPa range [14,32]. However, many ZrO_2 based dental glass-ceramics have H around 9 GPa and E higher than 120 GPa (up to 240 GPa for ytria-stabilized zirconia [33]) and are still used as dental prosthesis [34]. S. Galia et al. found that the mechanical strength of zirconia toughened mica GCs (containing 20 wt% YSZ) achieved a Vickers hardness of 9.2 GPa, an E of 125 GPa, and an indentation fracture toughness of 3.6 MPa $m^{1/2}$, which E was close to that for the developed GC [35].

The fracture strength measured using the B3B technique was 450 ± 40 MPa. The fracture toughness, K_{DTIC}, measured by the double-torsion technique, was 3.5 ± 0.5 MPa $m^{1/2}$.

Fig. 4(a) shows a laser confocal micrograph of a fractured surface. A typical topography of the fracture surface is illustrated in Fig. 4 (b), whereas Fig. 4 (c) shows the frequency distribution of fracture surface angles. There is a wide distribution that includes angles close to 90°, which indicates significant crack deflection. A pseudo-Voigt function P_V was fitted to the data and is also shown in Fig. 4 (c). From the calculated cumulative frequency (not shown), the median angle is 23.4°. This value is higher than for fully crystallized $Li_2O{\cdot}2SiO_2$, 18.7° [24], which shows similar fracture toughness.

Fig. 5 shows the thermal expansion curves of the parent glass and the GC. The average GC linear TEC is 13.6 × 10-6 °C-1 in the temperature range50–440 °C. This value is very close to that of the TEC of parent

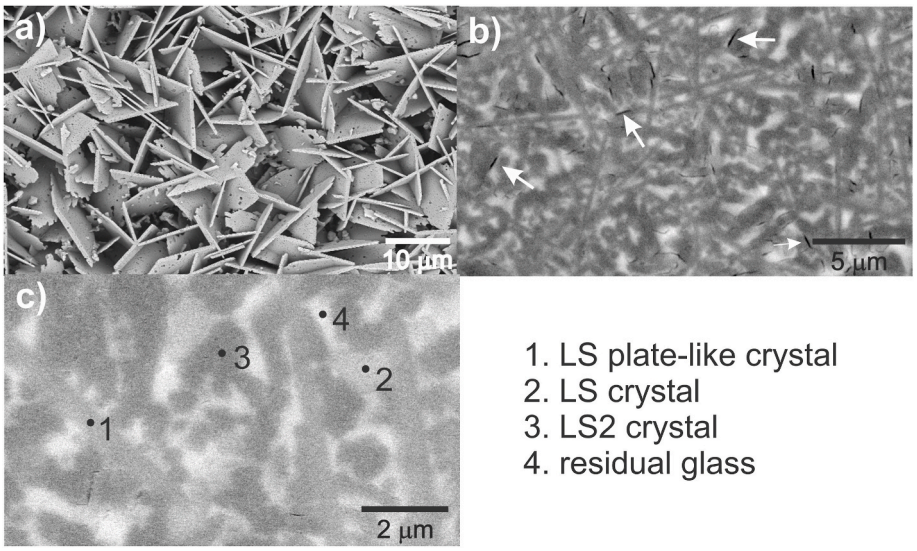

Fig. 2. SEM micrographs using backscattered electrons. a) Glass-ceramic polished and etched (HF 5%vol. for 10s) revealing a "house-of-cards" network of LS crystals of plate-like morphology; b) and c) glass-ceramic polished surface. White arrows in Fig. 2b indicate dark microcracks. In addition to other phases, some round LS crystals are also shown in Fig. 2c.

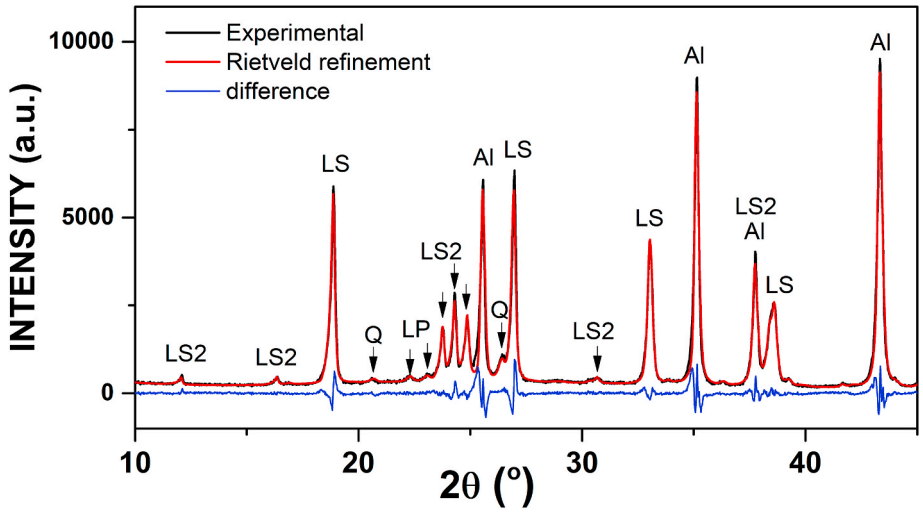

Fig. 3. XRD (red) and Rietveld refinement (residuals in blue) of the mixture of glass-ceramic and α-Al_2O_3 for quantification of the crystallized phases. The identified phases are: A - α-Al_2O_3; LS – Li_2SiO_3; LS2 – $Li_2Si_2O_5$; LP – Li_3PO_4; Q - α-quartz.

glass, 14 × 10 -6 °C-1, in the same temperature range. The GC TEC increases as the temperature increases, reaching 27 × 10-6 °C-1 in the temperature interval 510–710 °C. This large change in TEC is associated with the Tg of the residual glass phase, which is 510 °C, i.e., it is 67 °C higher than the Tg of the parent glass. The softening point of the lithium metasilicate GC is 807 °C.

The residual strains along the unit cell directions ε_a, ε_b and ε_c measured by XRD, and the average strain and residual stresses at the different phases are shown in Table 1. The values of E are 124 GPa and 120 GPa for the Li_2SiO_3 and $Li_2Si_2O_5$ phases, respectively [36]. The Poisson ratios were assumed to be 0.24 and 0.19 for Li_2SiO_3 and $Li_2Si_2O_5$, respectively. The residual strains were anisotropic. The *a*- and *c*-directions of the Li_2SiO_3 phase are under compression, whereas the *b*-direction is under tension. For the $Li_2Si_2O_5$ phase, the *a*- and *b*-directions are under tension, and the *c*-direction is under compression. The measured average residual stresses are quite low: +60 ± 20 MPa (tensile) for the major phase Li_2SiO_3, and -60 ± 50 MPa (compressive) for the $Li_2Si_2O_5$ crystals.

The percentage of total transmittance, T_t%, as a function of wavelength for the lithium metasilicate GC developed in this work and for other commercial GCs are shown in Fig. 6. The T_t% of commercial GCs increase with wavelength, whereas our new GC shows a T_t% approximately constant up to 700 nm (from 27% to 32%). Considering the T_t% measured at 555 nm, the developed GC and Press A1 HT show approximately the same value (30%), whereas the Press A3 LT presents 27%. Press A3 MO reach only 22% in T_t% measured at 555 nm. This result was expected because this material has the highest level of opacity among the tested commercial samples [14,37]. Therefore, the transmittance of the developed lithium metasilicate GC is comparable to that of Press A1 HT at 555 nm, which are both more translucent than the Press A3 LT and Press A3 MO for wavelengths up to 700 nm.

To evaluate the machinability, a molar tooth was designed, and a sample was machined using a CAD/CAM restorative technique. As shown in Fig. 7(a), before machining, the lithium metasilicate GC was glued to a metallic support. Fig. 7(b) shows the final tooth. It was, thus, possible to obtain a tooth of high complexity, which indicates the reasonable machinability of the new GC and the feasibility of producing dental prosthesis by this process.

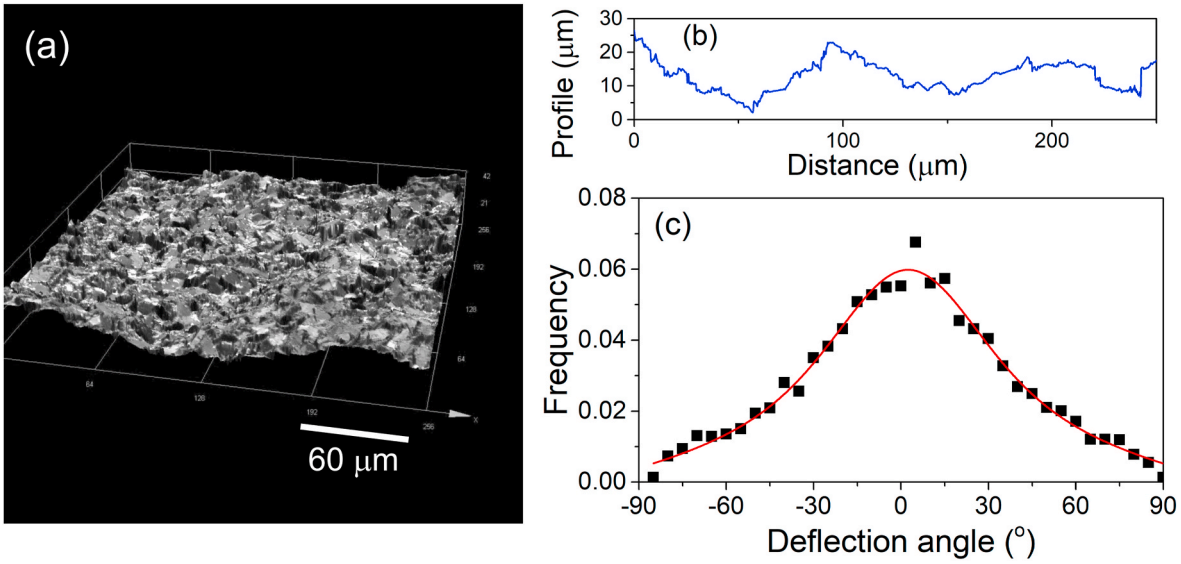

Fig. 4. (a) Optical laser confocal micrograph, (b) typical topography and (c) the frequency distribution with a pseudo-Voigt function fitted to the experimental data of a fracture surface of the lithium metasilicate glass-ceramic.

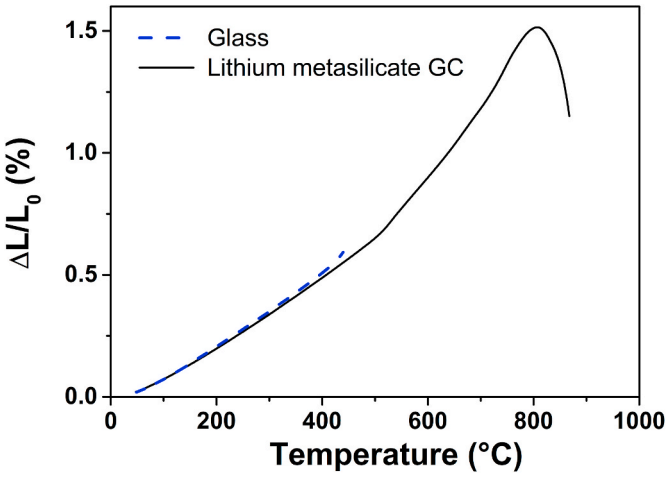

Fig. 5. Linear thermal expansion curves of the parent glass and lithium metasilicate glass-ceramic showing the T_g (510 °C) and the softening point (807 °C) of the residual glass.

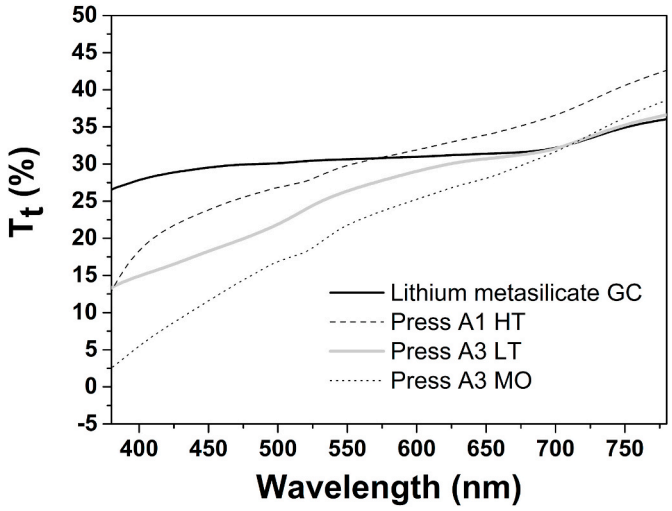

Fig. 6. Total light transmittance in percentage (T_t%) of the new lithium metasilicate glass-ceramic compared to commercial lithium disilicate glass-ceramics. (All samples were 0.95 ± 0.02 mm thick).

Table 1
Residual strains along the different crystallographic directions of the unit cell and average residual strains and stresses at the different phases as measured by XRD. The numbers in brackets are the standard deviation.

	ε_a (%)	ε_b (%)	ε_c (%)	$\bar{\varepsilon}$ (%)	$\bar{\sigma}_{exp}$ (MPa)
Li_2SiO_3	-0.0175(7)	0.1666(3)	-0.0654(2)	0.028(8)	60(20)
$Li_2Si_2O_5$	0.0014(8)	0.385(1)	-0.2170(6)	-0.03(3)	-60(50)

Finally, according to the dental standard ISO 6872 [29], the chemical durability after treatment with an acetic acid solution 4% vol. is 215 ± 30 μg/cm^2.

4. Discussion

4.1. Fracture toughness and strength

We were able to obtain a new type of lithium metasilicate GC with fracture strength of 450 ± 40 MPa (B3B) and K_{DTIC} of 3.5 ± 0.5 MPa m$^{1/2}$. The value of K_{DTIC} is somewhat higher than that of Ivoclar's IPS e.max CAD (3.1 ± 0.2 MPa m$^{1/2}$) measured by the same double-torsion technique [38]. According to Belli et al. [39], the fracture toughness of IPS e.max CAD and Celtra Duo A2 measured by single edge V-notched bending (SEVNB) are 2.3 ± 0.2 MPa m$^{1/2}$ and 1.7 ± 0.1 MPa m$^{1/2}$, respectively. We cannot compare these values directly with the current GC because they were measured by different techniques. Published values for other successful commercial GCs, measured by single edge V-notched bending (SEVNB) are: Macor (1.5 MPa m$^{1/2}$) [2,40], IPS e.max CAD (2.0–2.8 MPa m$^{1/2}$) [41,42] and IPS e.max Press (2.8–3.3 MPa m$^{1/2}$) [37,41,43]. However, we emphasize that these two methods - SEVNB and DTIC - do not yield the same value of fracture toughness.

Other bioactive and dental GCs have been reported to have a high fracture toughness (K_{IC}). The commercial bioactive Cerabone A/W GC, based on the MgO–CaO–SiO_2–P_2O_5 system, shows a fracture strength of 213 MPa measured by three-point bending and a K_{DTIC} of 2.6 MPa m$^{1/2}$ [44]. Its high strength and toughness were attributed to the crystallization of needle-like wollastonite crystals. Apatite-mullite GCs based on

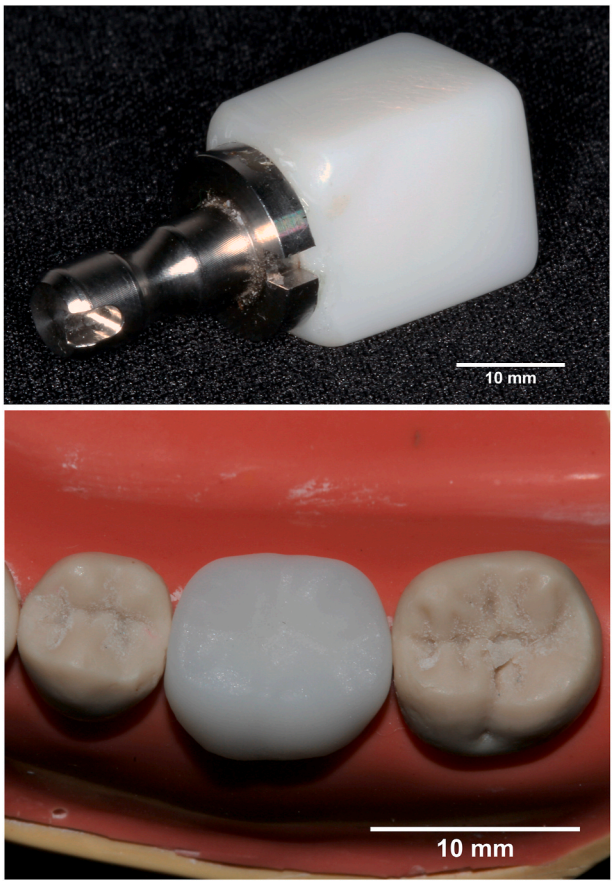

Fig. 7. (a) lithium metasilicate glass-ceramic prepared for machine milling; (b) molar tooth obtained.

the (2-x)SiO_2–xP_2O_5–Al_2O_3–CaO–yCaF_2 system have also been reported by Hill et al. [45]. They have K_{IC} values of 1.0–3.3 MPa $m^{1/2}$ and bending strength of 90–330 MPa. Other well-known bioactive GCs are the machinable Bioverit I (K_{IC} = 1.2–2.1 MPa $m^{1/2}$ and σ = 140–180 MPa) and Bioverit II (K_{IC} = 1.2–1.8 MPa $m^{1/2}$ and σ = 90–140 MPa), which mainly consist of elongated and "cabbage-head" mica crystals, respectively [46].

The dental LS2 GC IPS.Empress2 shows a maximum 3-point flexural strength of 400 MPa and a maximum K_{IC} of 3.3 MPa $m^{1/2}$ (single edge notched beam (SENB) test) [43]. These good mechanical properties result from a microstructure that also consists of acicular interlocked crystals.

Another GC with excellent mechanical properties is based on enstatite [47]. The presence of clinoenstatite results in a fracture strength of 200 MPa and a K_{IC} of 4.6 MPa $m^{1/2}$ (SENB/Chevron-notched beam/-Short bar). The main toughening mechanism was suggested to be the *clino → protoenstatite* phase transformation, which promotes crack deflection and fracture surface split due to cleavage. MgO–Al_2O_3–SiO_2 GCs also present excellent mechanical properties [48]. The crystallization of enstatite and karrooite, with acicular form, results in a fracture strength of 165 MPa (flexure test ASTM C-158-95B) and K_{IC} of 4.3 MPa $m^{1/2}$ measured by the short bar SENB method. The highest fracture toughness ever reported refers to a GC with fluorcanasite crystals [49]. Due to its lamellar structure, a fracture strength of 300 MPa and a K_{IC} of 5.0 MPa $m^{1/2}$ (SENB) were reported. This high toughness was attributed to the interlocking structure, cleavage splintering of the crystals and microcracking induced by the high thermal anisotropy.

Some of the toughening mechanisms reported above are likely to be active in the microstructure of our new lithium metasilicate GC, which shows an interlocked microstructure consisting of "house-of-cards" LS crystals. The fracture surface morphology presented in Figs. 2 and 4 indicates extensive cleavage leading to crack tilt and twist. This might be attributed to crack splintering due to cleavage of the LS crystals or along the crystal-glass interface, which results in extensive crack deflection. The median of the crack deflection calculated from Fig. 4(c) was 23.4°, which is even higher than that of a fully crystallized LS2 GC [24]. This higher crack deflection may be the result of the LS crystals as platelets, which produces more crack deflection than spheres, the form of LS2 crystals.

There are at least two models for calculating the toughening contribution of crack tilting and twisting of dispersed platelets in a matrix composite. In studies carried out by Faber and Evans [50] and Kotoul et al. [51], the tilt and twist angles are described as a function of the disk (particle) orientation in respect to the crack front and the presence of neighbor disks. The validity of these models is for low volume fraction composites.

To the best of our knowledge, there are no available models for GCs with high crystallized volume fraction. To estimate the contribution of crack tilting and twisting on the increase of fracture toughness for our GC, we used the frequency distribution, P_V, of the fracture surface angle fitted to the data in Fig. 4(c). Crack tilting and twisting induces modes II and III loading in the crack front. The increase in toughening G_C due to crack deflection is [51]:

$$G_C = \frac{G_m}{\langle G \rangle} G_{mC} \tag{3}$$

where G_{mC} is the critical energy release rate of the matrix and:

$$\frac{G}{G_m} = \cos^2\frac{\lambda}{2}\left(2\nu\sin^2\varphi + \cos^2\frac{\lambda}{2}\right)^2\cos^4\varphi + \cos^2\varphi\sin^2\frac{\lambda}{2}\cos^4\frac{\lambda}{2} + \frac{\cos^2\frac{\lambda}{2}\sin^2\varphi\cos^2\varphi}{1-\nu}\left(2\nu - \cos^2\frac{\lambda}{2}\right)^2 \tag{4}$$

where λ and φ are the tilt and twist angles, respectively. We assume that the function P_V is the same angle distribution function both for λ and φ and $\langle G \rangle / G_m$is:

$$\frac{\langle G \rangle}{G_m} = \frac{\int_{-\pi/2}^{\pi/2}\int_{-\pi/2}^{\pi/2} P_V(\lambda)P_V(\varphi)\frac{G}{G_m}d\lambda d\varphi}{\int_{-\pi/2}^{\pi/2}\int_{-\pi/2}^{\pi/2} P_V(\lambda)P_V(\varphi)d\lambda d\varphi} \tag{5}$$

where G/G_m is given by eq. (4). The integrals were performed numerically and the increase in toughness due to crack tilting and twisting, G_C/G_{mC}, is 2.83. Since $K_{IC}/K_{mIC} = \sqrt{G_C/G_{mC}}$, then $K_{IC} = 1.68\ K_{mIC}$, where K_{mIC} is the fracture toughness of the matrix without crack deflection. Therefore, we estimate that for our GC the increase in fracture toughness due to crack deflection is **68%**. This leads to a K_{mIC} of 2.08 MPa $m^{1/2}$ for a GC without crack deflection. This is approximately the same fracture toughness of IPS e.max CAD of 2.3 ± 0.2 MPa $m^{1/2}$ [39]. This value is within the range shown in Ivoclar's catalog for this material.

The interlocked microstructure obtained also improves the GC's strength. The commercial LS2 dental GCs present a microstructure having acicular interconnected crystals, which ensure their high strength. The 3-point bend flexural strength is 450 ± 53 MPa for IPS e.max CAD [52]. According to Wendler et al. [53], the IPS e.max CAD shows a characteristic fracture strength (σ_0) of 650 MPa in a B3B test of disc samples, and 460 MPa in a 4-point bending test. The B3B test yields higher values because the area under tensile stress is significantly smaller. The high strength and toughness of this new lithium metasilicate GC are primarily attributed to its "house-of-cards" microstructure. Another study [54] reported the biaxial strength for a stoichiometric LS2 GC by B3B with samples similar to this study. For f = 66%, the values were in the range of 210–250 MPa, which are lower than the strength value measured in this study.

It should be emphasized that Wendler et al. [53] reported an average value of 650 MPa (B3B) and 460 MPa (4-point bending) for the fracture strength of the commercial GC e.max.CAD, whereas the catalog value is "only" 360 MPa, as measured by the biaxial strength, Pin-on-3 balls test. This enormous difference in strength partially results from different sample polishing techniques, and part from the fact that, in each test type, the sample volume subjected to tensile stress is different. Thus, B3B tests typically result in higher strength values because the volume of material under tensile stress is minute, much smaller than on the Pin-on-3 balls or in a 4-point bending test.

The mechanical properties of a GC containing LS as a major phase is reported in Refs. [30]. A glass with 44%mol $CaSiO_3$ and 56%mol Li_2SiO_3 was heat-treated to obtain a GC containing 54%vol. Li_2SiO_3 had a crystal size of 8.5 μm and 32%vol. $CaSiO_3$ surrounded the LS crystals. This GC presented a $K_{DTIC} = 2.3 \pm 0.5$ MPa $m^{1/2}$ and biaxial strength (B3B) of 270 ± 20 MPa; these mechanical properties are also considerably lower than those obtained in this study. A likely explanation is, thus, the difference in the crystal morphology of the LS phase obtained in Refs. [30] when compared to the interlocked plate-like LS microstructure obtained in this work.

When designing a new product, both fracture strength, σ_f, and fracture toughness must be taken into account and be analyzed together. For the sake of comparison, the σ_f and K_{IC} of several GCs were compiled in Fig. 8, where we plotted the maximum values of K_{IC} and σ_f reported for each GC group. Theoretically, fracture strength is expected to increase with K_{IC}. K_{IC} is a material property that only depends on the material's microstructure and the measurement technique, whereas the fracture strength also depends on the sample size, surface condition, etc.

Dental GCs have superior properties compared to human dentin (K_{IC} ~ 1.0–2.0 MPa $m^{1/2}$ and σ = 230–305 MPa) and to natural internal enamel (K_{IC} ~ 1.0–4.0 MPa $m^{1/2}$ and σ = 260–290 MPa) [3,55,56]. Their fracture toughness varies from 2 to 3 MPa $m^{1/2}$, whereas their fracture strengths lie in the range of 250–450 MPa. Other tough (non-dental) GCs display even higher toughness, between 4.2 and 4.8 MPa $m^{1/2}$. However, their fracture strength is relatively low, approximately 200 MPa, and these values also depend on sample preparation conditions and measurement methods. In summary, the GC reported in this work seems to exhibit one of the best toughness-to-strength combinations.

Thermal residual stresses are intrinsic to GCs due to the different thermal expansion coefficients of crystallized phases and the residual glass. They are an important cause of microcracking during cooling or under external stresses [24,25,36,57,58]. The average residual stresses measured by XRD were +60 ± 20 (tensile) MPa for the LS phase and -60 ± 50 MPa (compressive) for the LS2 phase. Considering the errors in these measurements, the residual stress in our GC is very low, close to zero. The main reason is probably stress relief caused by the microcracking observed in Fig. 2(b).

From the measurements of the average TEC of the GC and the crystallized volume fraction of each phase, it is possible to estimate the TEC of the residual glass assuming a rule of mixture. The average TECs of LS is 13.6 × 10^{-6} °C^{-1}, LS2 is 10.4 × 10^{-6} °C^{-1}, Li_3PO_4 is 14.1 × 10^{-6} °C^{-1} and α-SiO_2 is 13 × 10^{-6} °C^{-1} [36,59]. Using the Sciglass® software and the chemical composition, the estimated TEC of the residual glass is 12.2 × 10^{-6} °C^{-1}. The microcracking observed in Fig. 2(b) is observed in the residual glass/LS2 crystal interface. Its origin is attributed to the different TECs of the residual glass and the crystals. It is important to point out that the LS2 crystal is highly anisotropic (α_a = 13.3 × 10^{-6} °C^{-1}, α_b = 6.5 × 10^{-6} °C^{-1}, α_c = 9.6 × 10^{-6} °C^{-1}) [36].

Another possible cause of cracking of the residual glass could be the beta-to-alpha-quartz transition, which occurs on the cooling path at ~450 °C, well below the T_g of the residual glass. The key issue is that these cracks likely decrease the macroscopic strength of the glass-ceramic. Despite this fact, it is still quite high.

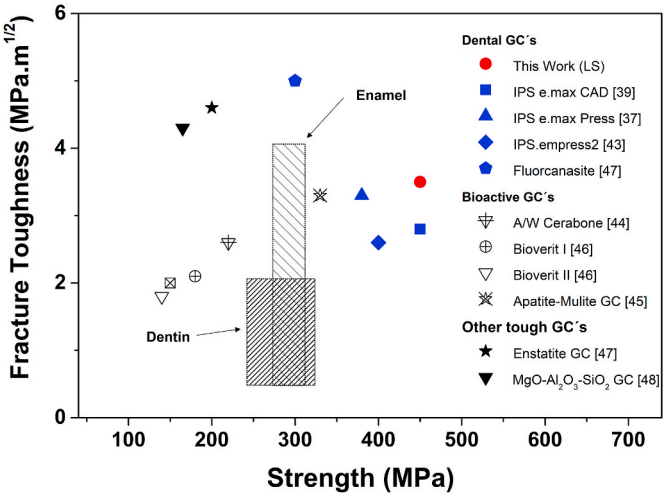

Fig. 8. Fracture toughness versus fracture strength of different types of tough glass-ceramics, including dental glass-ceramics. As the toughness and strengths were measured by different techniques, they cannot be directly compared. This figure only shows the overall "ball park" of these two properties.

4.2. Transmittance

Translucency is a key characteristic for dental GCs, and Tt% is an accurate and sensitive measurement to characterize the translucency in GCs with low and high opacity [60]. The obtained values of Tt% for the commercial LS2 GCs agree reasonably well with the results of Harada et. al., who reported 27% in Tt% at 555 nm to IPS e.max CAD LT [61]. The developed lithium metasilicate GC has a translucency comparable to that of Press A1 HT, and it is more translucent than that of Press A3 LT and Press A3 MO.

Considering the crystalline phases in the developed lithium metasilicate GC, the mean refractive index is around 1.55 for lithium disilicate; and is approximately 1.57 for lithium metasilicate [62]. The Li_3PO_4 crystal has a mean refractive index of 1.59 [63] and α-quartz has a mean refractive index of 1.54 [64], but these last two are minor phases in this GC. The refractive index of the residual glass estimated by the Sciglass® software is approximately 1.59. Therefore, the difference in refractive index between the residual glass and the main crystalline phases is approximately 0.04. This value is sufficiently low to yield low scattering and reasonable translucency. Therefore, with respect to translucency, the developed lithium metasilicate GC can be considered appropriate for dental application.

4.3. Machinability

The lithium metasilicate GC is indeed machinable, as shown by a molar tooth in Fig. 7 (b). Boccaccini [65] proposed a parameter for estimating the machinability of GCs, called brittleness index (B), which is the ratio of the hardness to the fracture toughness. According to Boccaccini, for a GC to be machinable, its brittleness index should be lower than 4.3 $\mu m^{-1/2}$. Considering the values of hardness and fracture toughness of our new GC, its brittleness index is approximately 2 $\mu m^{-1/2}$, which indeed indicates its machinability. However, these approximate estimates must still be compared with the actual values of commercial GCs for a better assessment of the actual degree of machinability of this new material.

4.4. Chemical durability

Considering the chemical durability and the fracture strength of the GC, according to ISO 6872 [29], the developed lithium metasilicate GC fulfills the requirements (ISO Class 3B) and can be accordingly indicated for partially or fully covered substructures for single-unit anterior or

posterior prostheses and for three-unit prostheses not involving molar restoration adhesively or non-adhesively cemented. However, the chemical durability of this new GC must still be improved to meet the necessary requirements to be applied as a monolithic ceramic for single-unit anterior or posterior prostheses and for three-unit prostheses not involving molar restoration adhesively or non-adhesively cemented (ISO Class 3A), where a value below 100 μg/cm^2 is required.

Finally, it should be mentioned that we could indeed produce glass samples as large as 12 × 12 × 60 mm^3, however in some cases a few crystals spontaneously precipitated on the cooling path. Therefore, for large scale production, the glass-forming ability (GFA) of this material must still be improved. On the other hand, addition of certain oxides, such as alumina and zirconia will likely improve both the chemical durability and GFA. These ideas warrant further research.

5. Conclusions

We developed a new GC containing approximately 50% vol. $LiSiO_3$ as the major phase, 12% vol. $LiSi_2O_5$, plus Li_3PO_4 and α-quartz as secondary phases dispersed in 34% vol. residual glass. Its chemical durability, 215 ± 30 μg/cm^2 (ISO 6872), is still above the standard for uncoated use, but enough for coated uses. We believe this property could be improved via small changes in the chemical composition and thermal treatment. This novel lithium metasilicate-based GC has a house-of-cards microstructure of randomly dispersed plate-like crystals that leads to superior mechanical properties: a high fracture toughness (K_{IDT} = 3.5 MPa m$^{1/2}$) and B3B strength (450 MPa), and machinability. It is also translucent.

Overall, these combined characteristics indicate that the newly developed glass-ceramic fulfills the most important requirements of the ISO 6872 standard for covered substructures. It is, thus, a promising starting material for dental restorative applications, which however should still be optimized regarding its glass-forming ability, chemical durability, and machinability.

Declaration of competing interest

The authors declare that they have no known competing financial interests or personal relationships that could have appeared to influence the work reported in this paper.

Acknowledgments

The authors are grateful to Arotec/Olympus for the laser confocal microscopy measurements and C-LABMU/UEPG. (FINEP/CNPq/CAPES/Fundação Araucária) for the use of the research facilities. We would also like to thank Dr. C. M. Lepienski for the instrumented indentation tests, Dr. Robson Ferrari Muniz for the transmittance analysis and Dr. Kei Maeda for his valuable suggestions in after reading the manuscript. The National Council for Scientific and Technological Development (CNPq – process 104429/2019-4) for the financial support. Funding by the São Paulo Research Foundation – Fapesp – process 2013/ 07793-6 is fully appreciated.

References

[1] J. Deubener, M. Allix, M.J. Davis, A. Duran, T. Höche, T. Honma, T. Komatsu, S. Krüger, I. Mitra, R. Müller, S. Nakane, M.J. Pascual, J.W.P. Schmelzer, E. D. Zanotto, S. Zhou, Updated definition of glass-ceramics, J. Non-Cryst. Solids 501 (2018) 3–10, https://doi.org/10.1016/j.jnoncrysol.2018.01.033.
[2] G.H. Höland, Wolfram, Glass- Beall, Ceramic Technology, second edi, John Wiley & Sons, Inc., Hoboken, New Jearsey, USA, 2012.
[3] M. Montazerian, E.D. Zanotto, Bioactive and inert dental glass-ceramics, J. Biomed. Mater. Res. 105 (2017) 619–639, https://doi.org/10.1002/jbm.a.35923.
[4] D.J. Fasbinder, Computerized technology for restorative dentistry, Am. J. Dent. 26 (2013) 115–120.
[5] W.H. Mörmann, The evolution of the CEREC system, J. Am. Dent. Assoc. 137 (2006) 7–13, https://doi.org/10.14219/jada.archive.2006.0398.
[6] S. Schultheis, J.R. Strub, T.A. Gerds, P.C. Guess, Monolithic and bi-layer CAD/CAM lithium-disilicate versus metal-ceramic fixed dental prostheses: comparison of fracture loads and failure modes after fatigue, Clin. Oral Invest. 17 (2013) 1407–1413, https://doi.org/10.1007/s00784-012-0830-1.
[7] T.F. Zesewitz, A.W. Knauber, F.P. Northdurft, Fracture resistance of a selection of full-contour all-ceramic crowns: an in vitro study, Int. J. Prosthodont. (IJP) 27 (2014) 264–266, https://doi.org/10.11607/ijp.3815.
[8] K.A. Malament, G. Grossman, D. Ph, The cast glass-ceramic restoration, J. Prosthet. Dent 57 (1987) 674–683, https://doi.org/10.1016/0022-3913(87)90362-3.
[9] T. Miyazaki, Y. Hotta, CAD/CAM systems available for the fabrication of crown and bridge restorations, 97-106, https://doi.org/10.1111/j.1834-7819.2010.01300.x, 2011.
[10] R.W.K. Li, T.W. Chow, J.P. Matinlinna, Ceramic dental biomaterials and CAD/CAM technology: state of the art, J. Prosthodont. Res. 58 (2014) 208–216, https://doi.org/10.1016/j.jpor.2014.07.003.
[11] W. Höland, V. Rheinberger, E. Apel, C. van't Hoen, Principles and phenomena of bioengineering with glass-ceramics for dental restoration, J. Eur. Ceram. Soc. 27 (2007) 1521–1526, https://doi.org/10.1016/j.jeurceramsoc.2006.04.101.
[12] L.H. Silva, E. Lima, R.B. de P. Miranda, S.S. Favero, U. Lohbauer, P.F. Cesar, Dental ceramics: a review of new materials and processing methods, Braz. Oral Res. 31 (2017) 133–146, https://doi.org/10.1590/1807-3107BOR-2017.vol31.0058.
[13] R. Fabian Fonzar, M. Carrabba, M. Sedda, M. Ferrari, C. Goracci, A. Vichi, Flexural resistance of heat-pressed and CAD-CAM lithium disilicate with different translucencies, Dent. Mater. 33 (2017) 63–70, https://doi.org/10.1016/j.dental.2016.10.005.
[14] e IPS, (n.d max CAD. http://www.ivoclarvivadent.com/en/p/all/all-ceramics/ips-emax-system-technicians/ips-emax-cad/ accessed September 13, 2019.
[15] R.B. Larson, C. Allen, Von Dreele, General structure analysis system (GSAS), 2004. Report LAUR 86–748.
[16] B.H. Toby, EXPGUI, a graphical user interface for GSAS, J. Appl. Crystallogr. 34 (2001) 210–213.
[17] A.A. Coelho, TOPAS and TOPAS-Academic: an optimization program integrating computer algebra and crystallographic objects written in C++, J. Appl. Crystallogr. 51 (2018) 210–218, https://doi.org/10.1107/S1600576718000183.
[18] G.M. Oliver, W.C. Pharr, An improved technique for determining hardness and elastic modulus using load and displacement sensing indentation experiments, J. Mater. Res. 7 (1992) 1564–1583, https://doi.org/10.1557/JMR.1992.1564.
[19] R. Danzer, W. Harrer, P. Supancic, T. Lube, Z. Wang, A. Börger, The ball on three balls test-Strength and failure analysis of different materials, J. Eur. Ceram. Soc. 27 (2007) 1481–1485, https://doi.org/10.1016/j.jeurceramsoc.2006.05.034.
[20] A. Börger, P. Supancic, R. Danzer, The ball on three balls test for strength testing of brittle discs: stress distribution in the disc, J. Eur. Ceram. Soc. 22 (2002) 1425–1436, https://doi.org/10.1016/j.jeurceramsoc.2003.10.035.
[21] A.G. Evans, A method for evaluating the time-dependent failure characteristics of brittle materials - and its application to polycrystalline alumina, J. Mater. Sci. 7 (1972) 1137–1146, https://doi.org/10.1007/BF00550196.
[22] D.P. Williams, A.G. Evans, A simple method for studying slow crack growth, J. Test. Eval. 1 (1973) 264–270, https://doi.org/10.1520/JTE10015J.
[23] A. Shyam, E. Lara-Curzio, The double-torsion testing technique for determination of fracture toughness and slow crack growth behavior of materials: a review, J. Mater. Sci. 41 (2006) 4093–4104, https://doi.org/10.1007/s10853-005-5553-0.
[24] F.C. Serbena, I. Mathias, C.E. Foerster, E.D. Zanotto, Crystallization toughening of a model glass-ceramic, Acta Mater. 86 (2015) 216–228, https://doi.org/10.1016/j.actamat.2014.12.007.
[25] F.C. Serbena, E.D. Zanotto, Internal residual stresses in glass-ceramics: a review, J. Non-Cryst. Solids 358 (2012) 975–984, https://doi.org/10.1016/j.jnoncrysol.2012.01.040.
[26] F.C. Serbena, V.O. Soares, O. Peitl, H. Pinto, R. Muccillo, E.D. Zanotto, Internal residual stresses in sintered and commercial low expansion Li 2O-Al2O3-SiO2 Glass-Ceramics, J. Am. Ceram. Soc. 94 (2011) 1206–1214, https://doi.org/10.1111/j.1551-2916.2010.04220.x.
[27] International commission on illumination, CIE S 017-2011 International lighting vocabulary (n.d.), http://cie.co.at/.
[28] Japanese Standards Association, JIS Z 8113-1998 Lighting vocabulary (n.d.), www.jsa.or.jp. accessed May 21, 2020.
[29] International Organization for Standardization, dentistry—ceramic materials, 2015. ISO 6872:2015.
[30] G.G. Santos, F.C. Serbena, V.M. Fokin, E.D. Zanotto, Microstructure and mechanical properties of nucleant-free Li2O-CaO-SiO2 glass-ceramics, Acta Mater. 130 (2017) 347–360, https://doi.org/10.1016/j.actamat.2017.03.010.
[31] O. Peitl, E.D. Zanotto, F.C. Serbena, L.L. Hench, Compositional and microstructural design of highly bioactive P 2O 5-Na 2O-CaO-SiO 2 glass-ceramics, Acta Biomater. 8 (2012) 321–332, https://doi.org/10.1016/j.actbio.2011.10.014.
[32] B.T.W. Leung, J.K.H. Tsoi, J.P. Matinlinna, E.H.N. Pow, Comparison of mechanical properties of three machinable ceramics with an experimental fluorophlogopite glass ceramic, J. Prosthet. Dent 114 (2015) 440–446, https://doi.org/10.1016/j.prosdent.2015.02.024.
[33] H. Sato, K. Yamada, G. Pezzotti, M. Nawa, S. Ban, Mechanical properties of dental sandblasting and heat treatment zirconia ceramics, Changed with 27 (2008) 408–414.
[34] L. Fu, H. Engqvist, W. Xia, Glass-ceramics in dentistry: a review, Materials 13 (2020), https://doi.org/10.3390/ma13051049.
[35] S. Gali, K. Ravikumar, B.V.S. Murthy, B. Basu, Zirconia toughened mica glass ceramics for dental restorations, Dent. Mater. (2018) 1–10, https://doi.org/10.1016/j.dental.2018.01.009.

[36] M.O.C. Villas-Boas, F.C. Serbena, V.O. Soares, I. Mathias, E.D. Zanotto, Residual stress effect on the fracture toughness of lithium disilicate glass-ceramics, J. Am. Ceram. Soc. 103 (2020) 465–479, https://doi.org/10.1111/jace.16664.
[37] e IPS, Max Press, n.d, http://www.ivoclarvivadent.com/en/p/all/products/all-ceramics/ips-emax-technicians/ips-emax-press. accessed September 13, 2019.
[38] F. Zhang, H. Reveron, B.C. Spies, B. Van Meerbeek, J. Chevalier, Trade-off between fracture resistance and translucency of zirconia and lithium-disilicate glass ceramics for monolithic restorations, Acta Biomater. 91 (2019) 24–34, https://doi.org/10.1016/j.actbio.2019.04.043.
[39] R. Belli, M. Wendler, A. Petschelt, T. Lube, U. Lohbauer, Fracture toughness testing of biomedical ceramic-based materials using beams, plates and discs, J. Eur. Ceram. Soc. 38 (2018) 5533–5544, https://doi.org/10.1016/j.jeurceramsoc.2018.08.012.
[40] Macor Machinable glass-ceramic for industrial applications (n.d.), https://www.corning.com/in/en/products/advanced-optics/product-materials/specialty-glass-and-glass-ceramics/glass-ceramics/macor.html. accessed September 13, 2019.
[41] R. Belli, M. Wendler, J.I. Zorzin, U. Lohbauer, Practical and theoretical considerations on the fracture toughness testing of dental restorative materials, Dent. Mater. 34 (2018) 97–119, https://doi.org/10.1016/j.dental.2017.11.016.
[42] E. Homaei, K. Farhangdoost, J.K.H. Tsoi, J.P. Matinlinna, E.H.N. Pow, Static and fatigue mechanical behavior of three dental CAD/CAM ceramics, J. Mech. Behav. Biomed. Mater. 59 (2016) 304–313, https://doi.org/10.1016/j.jmbbm.2016.01.023.
[43] W. Höland, M. Schweiger, M. Frank, V. Rheinberger, A comparison of the microstructure and properties of the IPS Empress®2 and the IPS Empress® glass-ceramics, J. Biomed. Mater. Res. 53 (2000) 297–303, https://doi.org/10.1002/1097-4636(2000)53:4<297::aid-jbm3>3.0.co;2-g.
[44] T. Kokubo, S. Ito, M. Shigematsu, S. Sakka, T. Yamamuro, Mechanical properties of a new type of apatite-containing glass-ceramic for prosthetic application, J. Mater. Sci. 20 (1985) 2001–2004, https://doi.org/10.1007/BF01112282.
[45] R.G. Hill, Bioactive glass–ceramics, in: P. Ducheyne (Ed.), Compr. Biomater. Vol. 1 Met. Ceram. Polym. Biomater., first ed., Elsevier, Netherlands, 2011, pp. 181–186.
[46] M. Montazerian, E. Dutra Zanotto, History and trends of bioactive glass-ceramics, J. Biomed. Mater. Res. 104 (2016) 1231–1249, https://doi.org/10.1002/jbm.a.35639.
[47] G.H. Beall, Chain silicate glass-ceramics, J. Non-Cryst. Solids 129 (1991) 163–173, https://doi.org/10.1016/0022-3093(91)90092-K.
[48] G.H. Beall, Refractory glass-ceramics based on alkaline earth aluminosilicates, J. Eur. Ceram. Soc. 29 (2009) 1211–1219, https://doi.org/10.1016/j.jeurceramsoc.2008.08.010.
[49] K.J. Anusavice, N.Z. Zhang, Chemical durability of dicor and fluorocanasite-based glass-ceramics, J. Dent. Res. 77 (1998) 1553–1559, https://doi.org/10.1177/00220345980770071101.
[50] K.T. Faber, A.G. Evans, Crack deflection processes–I. Theory, Acta Metall. 31 (1983) 565–576, https://doi.org/10.1016/0001-6160(83)90046-9.
[51] M. Kotoul, J. Pokluda, P. Šandera, I. Dlouhý, Z. Chlup, A.R. Boccaccini, Toughening effects quantification in glass matrix composite reinforced by alumina platelets, Acta Mater. 56 (2008) 2908–2918, https://doi.org/10.1016/j.actamat.2008.02.024.
[52] S.J. Kwon, N.C. Lawson, E.E. McLaren, A.H. Nejat, J.O. Burgess, Comparison of the mechanical properties of translucent zirconia and lithium disilicate, J. Prosthet. Dent 120 (2018) 132–137, https://doi.org/10.1016/j.prosdent.2017.08.004.
[53] M. Wendler, R. Belli, A. Petschelt, D. Mevec, W. Harrer, T. Lube, R. Danzer, U. Lohbauer, Chairside CAD/CAM materials. Part 2: flexural strength testing, Dent, Materials 33 (2017) 99–109, https://doi.org/10.1016/j.dental.2016.10.008.
[54] M.V. Senk, Effect of Crystalline Fraction and Crystal Size in Strength and Fracture Toughness of Lithium Disilicate Glass-Ceramics, State University of Ponta Grossa, Paraná, Brazil, 2017.
[55] N. Iwamoto, N.D. Ruse, Fracture toughness of human dentin, J. Biomed. Mater. Res. 66 (2003) 507–512, https://doi.org/10.1002/jbm.a.10005.
[56] Y.R. Zhang, W. Du, X.D. Zhou, H.Y. Yu, Review of research on the mechanical properties of the human tooth, Int. J. Oral Sci. 6 (2014) 61–69, https://doi.org/10.1038/ijos.2014.21.
[57] F.C. Serbena, G.P. Souza, E.D. Zanotto, J. Lumeau, L. Glebova, L.B. Glebov, Internal residual stresses in partially crystallized photo-thermo- refractive glass, J. Am. Ceram. Soc. 94 (2011) 671–674, https://doi.org/10.1111/j.1551-2916.2010.04372.x.
[58] O. Peitl, F.C. Serbena, V.R. Mastelaro, E.D. Zanotto, Internal residual stress measurements in a bioactive glass-ceramic using vickers indentation, J. Am. Ceram. Soc. 93 (2010) 2359–2368, https://doi.org/10.1111/j.1551-2916.2010.03717.x.
[59] J.A. Kosinsk, J.G. Gualtieri, A. Ballato, Thermal expansion of alpha quartz, in: Freq. Control. 1991. Proc. 45th Annu. Symp. on, IEEE, 1991, pp. 22–28.
[60] L.S. Spink, P. Rungruanganut, S. Megremis, J.R. Kelly, Comparison of an absolute and surrogate measure of relative translucency in dental ceramics, Dent. Mater. 29 (2013) 702–707, https://doi.org/10.1016/j.dental.2013.03.021.
[61] K. Harada, A.J. Raigrodski, K.H. Chung, B.D. Flinn, S. Dogan, L.A. Mancl, A comparative evaluation of the translucency of zirconias and lithium disilicate for monolithic restorations, J. Prosthet. Dent 116 (2016) 257–263, https://doi.org/10.1016/j.prosdent.2015.11.019.
[62] S. Buchner, M.B. Pereira, N.M. Balzaretti, Behavior of the refractive index of lithium disilicate glass ceramic processed at high pressure and high temperature, Opt. Mater. 34 (2012) 826–831, https://doi.org/10.1016/j.optmat.2011.11.018.
[63] I. Petousis, D. Mrdjenovich, E. Ballouz, M. Liu, D. Winston, W. Chen, T. Graf, T. D. Schladt, K.A. Persson, F.B. Prinz, Data Descriptor: high-throughput screening of inorganic compounds for the discovery of novel dielectric and optical materials, Sci. Data. 4 (2017) 1–12, https://doi.org/10.1038/sdata.2016.134.
[64] G. Ghosh, Dispersion-equation coefficients for the refractive index and birefringence of calcite and quartz crystals, Optic Commun. 163 (1999) 95–102, https://doi.org/10.1016/S0030-4018(99)00091-7.
[65] A.R. Boccaccini, Machinability and brittleness of glass-ceramics, J. Mater. Process. Technol. 65 (1997) 302–304, https://doi.org/10.1016/S0924-0136(96)02275-3.